Detailed Ignition Sequence Studied with a Fast Infrared Camera

Frédérick Marcotte[1], Eric Guyot[1,*], Alain deChamplain[2], Joël Jean[2], Alain Fossi[2], Sophie Ringuette[3]

[1]TELOPS, 100-2600 avenue St-Jean-Baptiste, Québec, QC, G2E6J5Canada
[2]Department of Mechanical Engineering, Combustion Laboratory, Université Laval
1065 avenue de la Médecine, Québec, QC, G1V 0A6 Canada
[3]Advanced Concepts Group, Defence Research and Development Canada - Valcartier
2459 de la Bravoure Road, Quebec, QC G3J 1X5Canada

Abstract

In an effort to better understand the interaction between the many parameters affecting ignition in a typical gas turbine combustor, a detailed study was made possible with a new facility available at Université Laval in collaboration with the companies Telops, Defence Research and Development Canada - Valcartier and Pratt & Whitney Canada. The installation is primarily focused on characterizing ignition process of different biofuel mixtures compared with the reference Jet-A fuel. The experimental setup is configured with a 75 mm (3 in) sapphire infrared optical access window looking directly into the combustion chamber. A Telops high speed and high performance infrared (IR) camera was used to characterize the ignition process. Large pulsations are observed before a steady combustion finally gets established for a successful ignition. It was possible to estimate the velocity of the expanding ignition volume that compared to typical flame speed measurements. Few IR videos and photos will be presented to visualize the full phenomena that would not be visible otherwise to the naked eye. Good correlation with temperature was also established to reflect the strong virtue of IR cameras to measure accurately emitted energy.

1. INTRODUCTION

In the coming years, biofuels will become strong contenders to replace petroleum based fuels. This growing interest is mainly driven by factors such as oil price, energy dependency and environmental concerns. However biofuel production yields, combustion efficiency and ignition properties are limited when compared to those of fossil base fuels. In an effort to better understand the interaction between the many parameters affecting biofuel ignition and combustion efficiency in a typical aircraft gas turbine combustor, direct observations were performed to visualize the interaction between the ignition kernel generated by a strong spark and the biofuel droplets reaching the highly energized and ionized region. This paper presents interesting transient measurements taken inside a combustion chamber using a high-speed and high-performance infrared imaging system.

2. EXPERIMENTAL SETUP

The installation is primarily dedicated to study the ignition behavior of different biofuel blended mixtures. The experimental setup is configured with a 75 mm (3 in) sapphire IR optical access window to look directly inside the combustion chamber. It allows direct observation of the interaction between the ignition kernel generated by a strong spark and the fuel droplets reaching the highly energized region. Equipped with a Telops FAST-IR 1500 high-speed infrared camera, it was then possible to look in the upstream

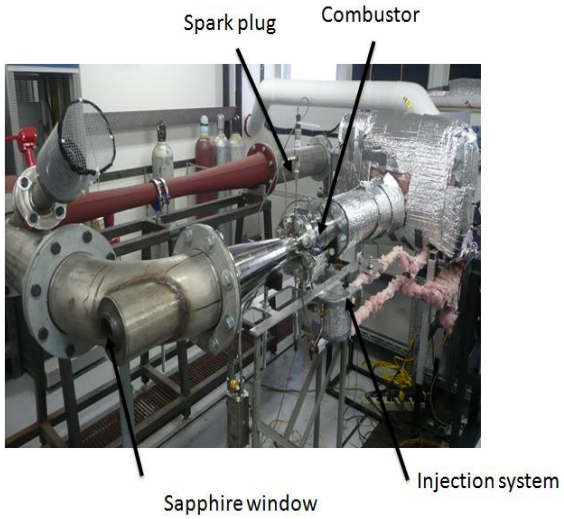

Figure 1: Experimental setup

* Corresponding Author: eric.guyot@telops.com

direction through this sapphire window directly inside the combustion chamber (Figure 1). The experimental setup and the infrared camera main control parameters are presented in Table 1.

Table 1 Control parameters for the infrared camera

Parameters	Unit	Value
Distance to combustion chamber	m	1.75
Camera frame rate -Spark analysis: -Gas droplets analysis: -Combustion analysis:	Hz	 5,000 3,000 10,000
Spatial resolution	Pixels	128 x 128
Camera FOV (HxV)	m	0.1 x 0.1
Camera sensitivity	mK	< 20

3. RESULTS AND DISCUSSION

Liquid biofuel blended mixtures in the form of injected fuel need to be characterized with respect to their ignition properties. Moreover, characterization must be performed under a large variety of ambient conditions. To characterize biofuel mixtures, the effect of the ignition spark and of the droplet size with distribution must be understood to enable the design of a reliable ignition system to respond to critical engine conditions such as ground cold start or altitude relight.

3.1 Ignition sparks analysis

The ignition system generates a high temperature ionized kernel from an arcing spark plug. The sparks are generated at a 3 Hz frequency. The IR results reveal an unprecedented capability for measuring key ignition characteristics. Figure 2 introduces a step by step sequence of temperature signature from the generated spark. The time difference between consecutive frames is 200 microseconds. On the top right section of images 1, 5, and 6 the artifact is caused by the low image contrast and by the camera field of view (FOV) looking a bit at the external combustion chamber wall. One can easily follow the dynamic progress of the spark lasting less than 800µs (frame #2 to frame #5). From these measurements, the maximum spark temperature, the temperature distribution, the spark active area and the spark transient progress can be studied (Figure 3). One can then derive the main impact of the spark physical characteristics evolving from ignition to steady-state combustion. For instance, the influence of the spark temperature and the active area or the physical position of the spark plug in the combustor as a function of fuel mixture and concentration can be readily optimized.

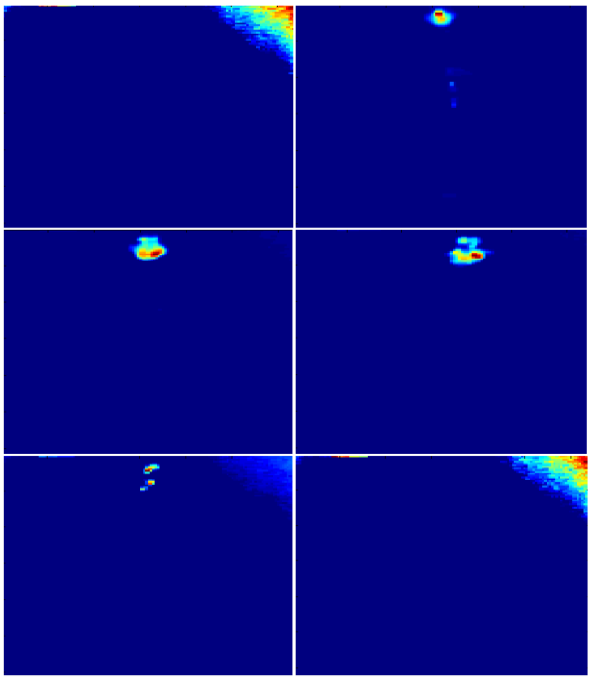

Figure 2: Spark temporal evolution

To demonstrate the reliability of the infrared camera temperature measurement, the maximum sparks temperatures were measured to be within the 300°C to 400°C range. The actual measured real ignition temperature of the fuel under test was measured to be 227°C in order to achieve a successful ignition.

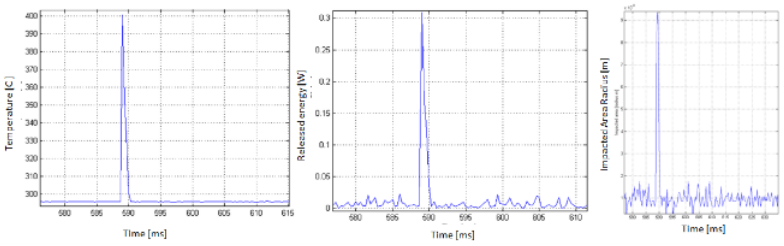

Figure 3: Ignition spark analysis, (Left) Maximum temperature. (Center) Spark released energy, (Right) Spark active area

3.2 Injection system analysis

In typical engine combustors fed with a liquid fuel spray, combustion instability is highly related to fuel droplet sizes and distribution. It is thus vital to understand the injection mechanisms of specific biofuels. This part of the combustion process can be directly optimized using a high-speed infrared imagery system. A good fuel injection system needs to spray uniformly and continuously the fuel into the combustion chamber. The fuel droplet sizes and

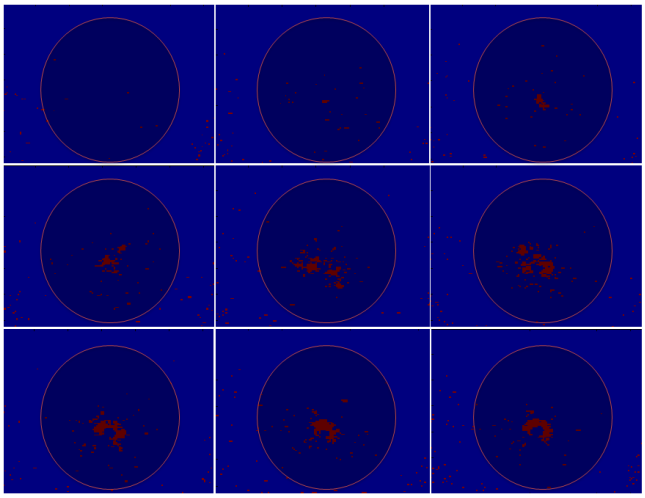

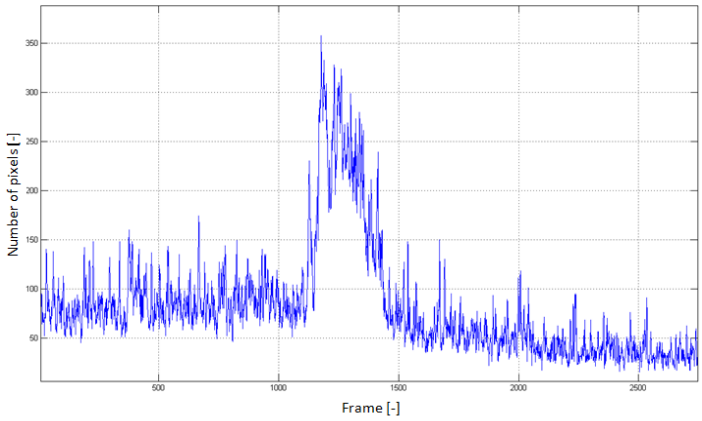

distribution resulting from the hollow cone spray produced by the fuel injector is key to the efficiency of the ignition and the combustion systems. Figure illustrates the temporal detection of fuel droplets during a typical transient fuel injection process. In steady-state mode (frame 7 to 9 in Fig. 5), fuel droplets are detected for roughly 100 pixels. The fuel droplet detection count then increases for no known reason to about 350 counts between frame 1200 and frame 1300. Then the behavior of the fuel injection process drastically changed and only 25 to 50 pixels detected as part of the injection process. Such behavior is an example of an anomaly that degrades combustion efficiency. When analyzing in more details the Figure 5 dynamic at the beginning of a fuel injection process inside the combustion chamber we can notice, the fuel droplets are not sprayed evenly and uniformly inside the combustion chamber (Red points in Figure 5). Most droplets are directed toward the bottom half of the combustor. An energy balance between the fraction of the spray that would have evaporated and burned could be associated to the rise in temperature in the specific area as discussed in the next section. This is a good example of how fast infrared imagery helps to understand and optimize the combustion process.

3.3 Combustion ignition

Finally, a fast thermal camera is useful to study the dynamic of a successful/unsuccessful ignition. A sub-

Figure 4: Fuel injection detection.

sampled sequence of images representing the transient ignition phase is shown in Figure 6. As expected and shown on the sequence, the maximum temperature of about 2 200 K stabilizes near the center of the combustor after shifting from the top where the high energy ignition kernel initiates combustion to gradually propagate to the middle under the influence of the conical spray injecting right in the center. Also the gas temperature quickly drops toward the combustor wall that is initially near ambient temperature. The total elapsed time between the first and the last image is about 100 milliseconds. Large pulsations are easily observed before the steady-state combustion finally gets established for a successful ignition. Figure 7 introduces the spatial temperature distribution approximately 400 milliseconds following ignition to indicate successful combustion with the resulting high temperature. The results from the measurements reveal a quasi-circular temperature distribution once the steady-state mode is established.

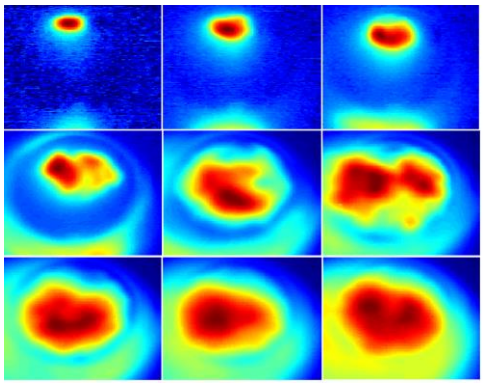

Figure 6: Transient ignition phases

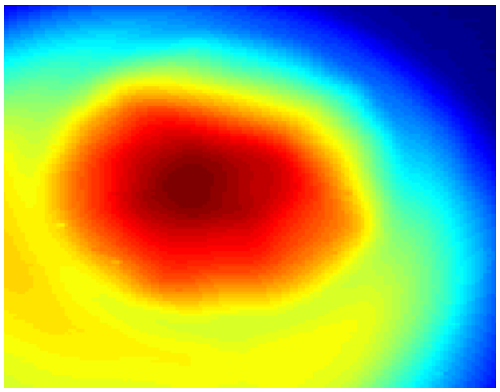

Figure 7: Steady-state successful combustion

Another interesting way to analyze the performance of the ignition process with the FAST-IR 1500 infrared camera in this dynamic high-energy application is to look at the progression of the maximum temperature and the total released energy resulting from the combustion active surface area. As shown in Figure 8, the user has direct access to the maximum temperature and can easily calculate the total emitted energy occurring during the combustion.

The energy emitted is equal to the pixel summation of the product of the spatial dimension (*IFOV*), corresponding to a given pixel field-of-view, and the temperature measured for each pixels considering the target emissivity ε and the Stefan Boltzmann constant.

$$E[W] = \sum_{pixelf=1}^{p} IFOV^2 \varepsilon \sigma \Delta T^4 \quad \frac{Signal}{6\left(NETD_{frame=1}^{10}\right)} = SNR, SNR > 5$$

This model assumes the target under measurement follows the gray body emission rules. (Mainly the emissivity is not spectrally structured). Summation is done for all pixels determined to be part of the impacted area according to a given signal to noise (SNR) ratio. A SNR > 5 is required in this experiment to get scientific grade detection. In fact, the total energy produced by the combustion process peaks at around 20 kW after approximately 0.8 second after steady-state is reached. Interesting features appear in both the energy and temperature temporal graphs. From this analysis, it is obvious to notice that the ignition was not successful following the first spark where temperature decreased before it would start to raise again. Two sparks were required to successfully initiate combustion. Also several peaks can be clearly distinguished during the transient phase. As presented in Figure 8, these peaks are not appearing randomly.

The most frequent peaks appear at a frequency of 3 Hz and 13 Hz. These frequencies correspond to the ignition spark frequency and to the air injection system inside the combustion chamber respectively. Even in steady-state mode these peaks are affecting the combustion process. The consequences are reduced combustion efficiency, increased noise, and the generation of potential instabilities inside the combustor.

High-speed infrared imaging also allows to compute the flow velocity profile resulting from an expending gas. An optical flow analysis method was used to estimate the directional velocities of the combustion flame and to study its ignition behavior. Both the velocities direction and amplitude are estimated. The resulting quantities form a vector field that informs very well on the evolution of the combustion throughout space and time.

The analyzed combustion sequence typically featured irregular motions that call for a flow estimation method that does not rely on some predetermined

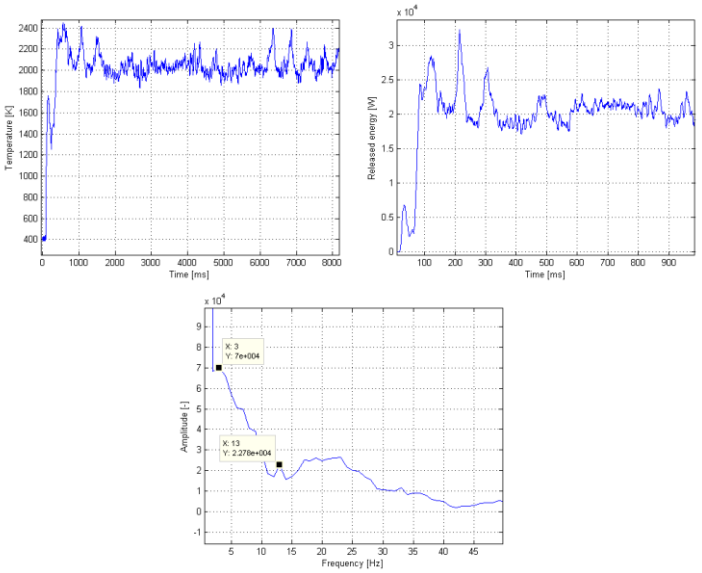

shape features or direction of motion. A scene-based radiance gradient method was chosen as it is well adapted to such highly dynamic and highly energetic sequences. According to the first law of thermodynamics, the energy entering and exiting a system must be constant. Thus, the chosen optical flow model assumes local conservation of intensity (radiance) between successive frames. Referring to a given pixel in the scene, the following constraint condition is then imposed on the image intensities $f(x, y, t)$:

$$f\left(x + v_x \Delta t, y + v_y \Delta t, t + \Delta t\right) = f(x, y, t) \quad \textbf{(1)}$$

where $v_x$and v_y are the velocity components in the x (horizontal) and y (vertical) axes respectively, and Δt is the elapsed time between successive frames. If one develops the right hand side of equation **(1)** into its Taylor series expansion and neglects the higher order terms, the following relation is obtained:

$$f(x + v_x\Delta t, y + v_y\Delta t, t + \Delta t) \approx f(x,y,t) + \frac{\partial f}{\partial x}v_x\Delta t + \frac{\partial f}{\partial y}v_y\Delta t + \frac{\partial f}{\partial t}\Delta t \quad \textbf{(2)}$$

It follows from the constraint equation **(1)** that:

$$\frac{\partial f}{\partial x}v_x + \frac{\partial f}{\partial y}v_y = -\frac{\partial f}{\partial t} = \vec{\nabla} f \cdot \vec{v}) \quad \textbf{(3)}$$

Consequently, the gradient constraint equation **(3)** must be solved for the velocities v_x and v_y. The system corresponding to equation **(3)** being underdetermined, a common way of solving it is by using the Lucas-Kanade algorithm [1][2]. This method assumes a locally constant velocity vector to solve equation **(3)** in a least-squares sense. The velocity vector $\vec{v} = v_x\vec{\imath}_x + v_y\vec{\imath}_y$ at position (x, y) is estimated by forming a 2x2 system of equations using neighbourhood pixels p around the pixel of interest. The system to be solved is as follows:

$$\begin{bmatrix} \sum_{i\in p} w_i f_{xx}(i) & \sum_{i\in p} w_i f_{xy}(i) \\ \sum_{i\in p} w_i f_{yx}(i) & \sum_{i\in p} w_i f_{yy}(i) \end{bmatrix} \begin{bmatrix} \mathrm{v_x} \\ \mathrm{v_y} \end{bmatrix} = - \begin{bmatrix} \sum_{i\in p} w_i f_{tx}(i) \\ \sum_{i\in p} w_i f_{ty}(i) \end{bmatrix} \quad \textbf{(4)}$$

where $f_{uv} = \frac{\partial f}{\partial u} \cdot \frac{\partial f}{\partial v}$ and w_i is a weighting window. The linear system of equation **(4)** is then solved for every pixel across the entire image. As illustrated in Figure 9, the gas velocity and direction of propagation can be calculated using this technique. For instance, points 1, 2 and 3 indicate interesting flow information where directional propagation can be shown from derived temperature gradients. Near point 1, the flow is directed toward the bottom right hand side of the combustor. When the flow reaches the lower section of the combustor (point 2) it starts rotating clockwise close to the combustor wall. Point 3 represents a punctual turbulent point that appears as a local minimum or maximum. The gas expansion velocity surrounding point 1 is [*U*, *V*] = [4.5, -5.88] m/s, where *U* is the horizontal and *V* is the vertical velocity. These results greatly help to understand the global and local thermodynamic behavior of the combustion process following a successful ignition.

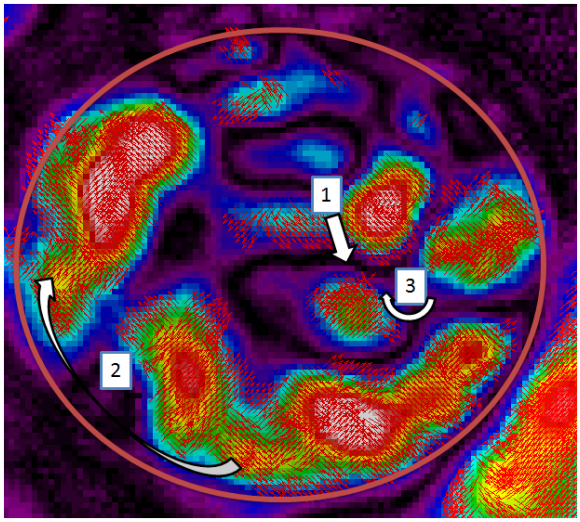

Figure 9: Combustion flow analysis

4. CONCLUSIONS

A highly turbulent combustion flow can be analyzed with a fast infrared imager. Important combustion characteristics such as the ignition spark, the injection system and the combustion transient and steady-state behavior can be measured dynamically. The fast infrared imagery analysis could lead to more efficient and stable combustor design. Moreover, the use of a Telops FAST-IR 1500 infrared camera for this particular application would help accelerate the design process to optimize ignition for all critical conditions encountered in typical aircraft combustors.

Acknowledgements

The authors would like to acknowledge the generous loan from Telops of their high speed infrared camera for the completion of this exploratory work.

References

[1] B.D. Lucas, T. Kanade, *An Iterative Image Registration Technique with an Application to Stereo Vision*, Proc. 7th (IJCAI1981), August 24-28, Vancouver B.C., pp. 674-679.

[2] J.L. Barron, D.J. Fleet, and S.S. Beauchemin, *Performance of Optical Flow Techniques*, (IJCV1994), 12(1):43-77

.

[3] E. P. Simoncelli, *Design of Multi-Dimensional Derivative Filters*, First IEEE Int'l Conf. on Image Processing, Austin Texas, vol. I, pages 790--793, November 1994.

[4]Jerold E. Marsden, Anthony J. Tromba, *Vector Calculus, Third Edition*,

[5]Frank P. Incropera, *Fundamentals of Heat and Mass Transfer*, Third edition